Geochemical Perspectives Letters

In situ redox control and Raman spectroscopic characterisation of solutions below 300 °C

I.-M. Chou[1*], R. Wang[1,2], J. Fang[1,3]

https://doi.org/10.7185/geochemlet.2135

Abstract

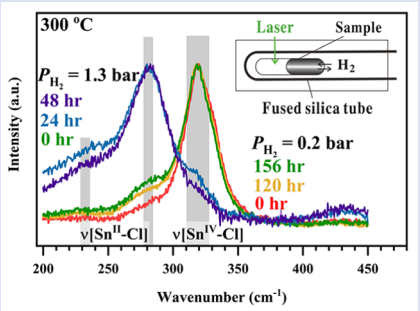

Redox reactions often occur and significantly affect many geological processes. To simulate redox reactions in low temperature (T < 400 °C) hydrothermal experiments, fused silica was used as a hydrogen membrane to impose an externally fixed H_2 pressure (P_{H_2}) on a fused silica capillary capsule (FSCC; 150 μm inner diameter, 375 μm outer diameter and ~6 mm long) to define the redox state of the sample in the FSCC. At 300 °C, it required less than 7 hours to reach osmotic equilibrium. In this study, a constant P_{H_2} was imposed on an FSCC, which originally contained a 0.5 *m* (mole/kg H_2O) $SnCl_4$ + 0.5 *m* HCl aqueous solution, at 300 °C and vapour saturation pressure. *In situ* Raman spectra of the sample solution collected at 300 °C show that the reduction rate of Sn^{IV} to Sn^{II} species increased substantially with an increase of 1.1 bar of P_{H_2}. We characterised precipitation and dissolution of cassiterite under various *P*-*T*-pH-P_{H_2} conditions and greatly increased our capabilities for performing rigorous hydrothermal experiments at temperatures below 400 °C, in which redox control is difficult to ensure without *in situ* approaches.

Received 19 July 2021 | Accepted 7 November 2021 | Published 2 December 2021

Introduction

Many geological processes are affected by the redox state of the system, particularly those involving multivalence elements. To simulate these processes in laboratories, several well established redox control techniques have been applied in hydrothermal experiments, including the double capsule (or oxygen buffer) (Eugster, 1957) and Shaw membrane techniques (Shaw, 1963). However, even after considerable refinements in the past six decades (Chou, 1987; Taylor *et al.*, 1992; Berndt *et al.*, 2002; Matthews *et al.*, 2003; Alex and Zajacz, 2020), these techniques cannot be applied at low temperatures (T < 400 °C) because the precious metal hydrogen membranes that are commonly used in these techniques, such as Pt or Ag-Pd alloys, are not effective at these *T*s (Chou, 1986).

To overcome this difficulty, other experimental techniques that do not require precious metal hydrogen membranes were developed (see Supplementary Information, SI). However, these methods may suffer from leakage of H_2 from the autoclave, contamination by the buffer materials and possibly slow reaction kinetics of the redox buffer at low *T*s. On the other hand, due to its high permeability to H_2, fused silica has been adopted as a hydrogen membrane for T < 400 °C hydrothermal experiments (Chou *et al.*, 2008; Shang *et al.*, 2009; Fang and Chou, 2021). A vacuumed FSCC has been employed as a hydrogen fugacity (fH_2) sensor, which was sealed together with a redox buffer (either Ni-NiO or Co-CoO) in an Au capsule and pressurised externally in a cold seal pressure vessel (CSPV) at 100 MPa and equilibrated between 250 and 400 °C (Fang and Chou, 2021). The H_2 pressures (P_{H_2}) equilibrated at elevated *P*-*T* conditions, calculated based on the ideal gas law from the P_{H_2} values measured from quenched FSCCs at room *T*, were in good agreement with those predicted from available thermodynamic data. However, *in situ* Raman spectroscopic measurements are not possible because neither Au nor CSPV are transparent. Nevertheless, this technique opens perspectives for simultaneous *in situ* measurements that will be tackled in the present study.

Before the use of optical cells (*e.g.*, hydrothermal diamond anvil cells [HDACs], HPOCs, FSCCs), the quench method was used in most hydrothermal experiments, and the interpretation of the observed quenched products was always a great challenge, especially when non-quenchable species were involved. For example, trisulfur ion (S_3^-) plays important role during the hydrothermal transport and mineralisation of gold, but it is stable only at elevated *P*-*T*s (Pokrovski and Dubrovinsky, 2011; Pokrovski and Dubessy, 2015; Pokrovski *et al.*, 2015).

Therefore, this study proposes a new design combining HPOC and FSCC optical cells with a quantitative Raman spectroscopic analysis technique to perform *in situ* redox control

1. CAS Key Laboratory of Experimental Study under Deep-sea Extreme Conditions, Institute of Deep-sea Science and Engineering, Chinese Academy of Sciences, Sanya, Hainan 572000, China
2. University of Chinese Academy of Sciences, Beijing 100871, China
3. Center of Deep Sea Research, Institute of Oceanology, Center for Ocean Mega-Science, Chinese Academy of Sciences, Qingdao 266071, China
* Corresponding author (email: imchou@idsse.ac.cn)

and spectroscopic analyses for hydrothermal experiments below 300 °C. The sample is loaded in an FSCC, which is exposed to and equilibrated with H_2 at two different fixed *P*s in an HPOC. A case study on Sn-Cl complexes using this design is also reported.

Experimental Procedure

A schematic diagram of the experimental setup is shown in Figure 1. Detailed descriptions of optical cell setup, sample preparation, experimental procedures, collection and processing of Raman spectra are given in SI.

Osmotic Equilibrium and *In Situ* Redox Control in an FSCC

To achieve *in situ* redox control in an FSCC at elevated *P-T* conditions, we determined the experimental duration required to reach osmotic equilibrium between the sample in an FSCC and the externally imposed H_2 pressure (P_{H_2}) in an HPOC at a fixed *T*. The experimental setup shown in Figure 1 was modified by replacing the solution-containing FSCC with a vacuumed FSCC (inner tube 1 in Fig. 2a) and inserting a short fused silica capillary tube with the same ID and OD as the FSCC, but with two ends open (inner tube 2 in Fig. 2a). *In situ* Raman spectra were collected from inner tube 1 at 300 °C, first at a P_{H_2} of 1.2 bar (0 to 470 min) and then reduced to 0.5 bar (480 to 1050 min); the representative spectra collected at 0 to 900 min are shown in Figure 2b. The peak heights of $Q_1(1)$ vibrations of H_2 (PH_{H_2}) as a function of time are shown in Figure 2c. Results show that approximately 300 minutes were required for the vacuumed FSCC to reach the externally imposed P_{H_2} of 1.2 bar, and approximately 400 minutes to achieve osmotic equilibrium when the external P_{H_2} was reduced to 0.5 bar.

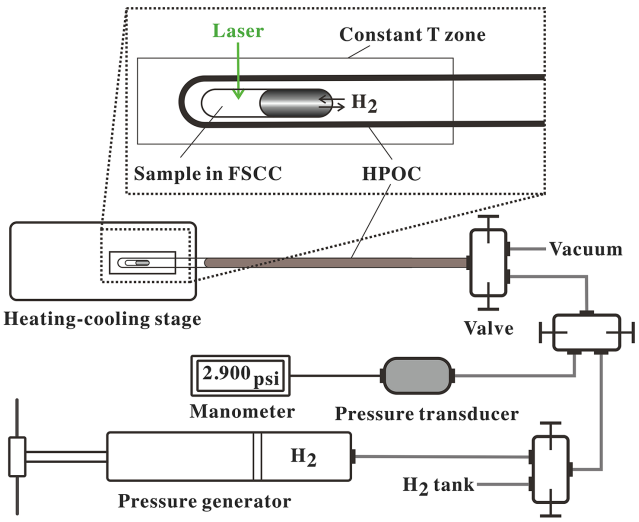

Figure 1 A schematic diagram showing the experimental setup. The sample solution was sealed in an FSCC, which was heated to a fixed *T* on a heating-cooling stage (Linkam CAP500) and exposed to a fixed external P_{H_2} either during heating or after reaching the target *T* (see SI for details).

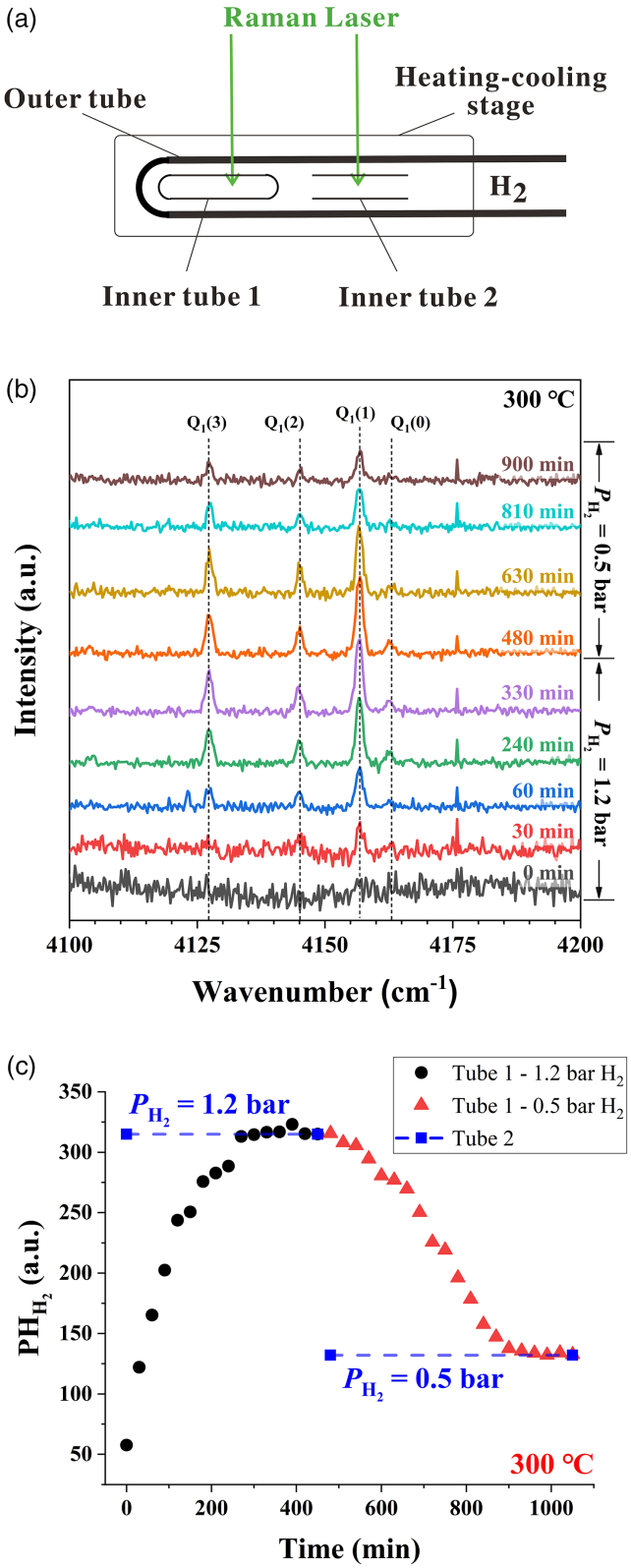

Figure 2 **(a)** A schematic diagram (modified from Fig. 1) showing the experimental setup for testing the osmotic equilibrium between P_{H_2} in an FSCC (inner tube 1) and externally imposed P_{H_2}. **(b)** Representative spectra collected from inner tube 1 under an externally imposed P_{H_2} of 1.2 bar (0 to 330 min) and 0.5 bar (480 to 900 min) with the four vibrational bands of H_2 marked. **(c)** Peak height of the $Q_1(1)$ vibrational band of H_2 (PH_{H_2}) measured in a vacuumed FSCC (inner tube 1) at various times after being externally imposed with a P_{H_2} of 1.2 bar (black dots) and then 0.5 bar (red triangles). The values of PH_{H_2} measured from inner tube 2 are shown by squares at 1.2 and 0.5 bar.

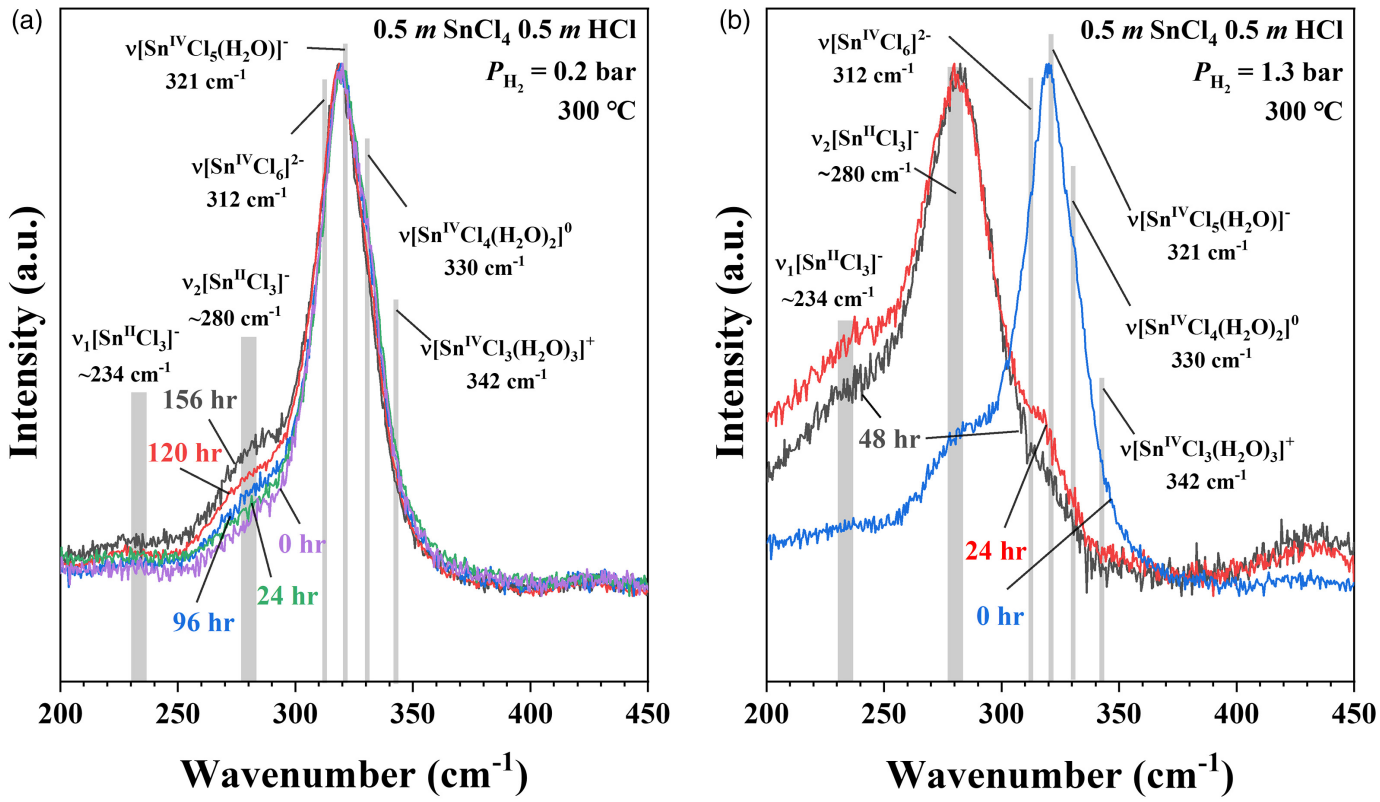

Figure 3 *In situ* Raman spectra of 0.5 *m* $SnCl_4$ + 0.5 *m* HCl solution (300 °C) in an FSCC under vapour saturated pressure after being exposed to **(a)** a P_{H_2} of 0.2 bar and then **(b)** 1.3 bar for various durations (shown in hours). The spectrum taken at 0 hr in **(b)** is the same spectrum taken at 156 hr in **(a)**. According to Schmidt (2018), the major Sn^{IV} species was $[Sn^{IV}Cl_5(H_2O)]^-$, which was reduced slowly to the Sn^{II} species, $[Sn^{II}Cl_3]^-$, under a P_{H_2} of 0.2 bar, as shown in **(a)**, and then quickly under a P_{H_2} of 1.3 bar, as shown in **(b)**. Each spectrum was collected for 200 s with 3 accumulations. The vertical gray lines were taken from Schmidt (2018), showing Raman peak positions of various Sn-Cl species at ambient *P-T* conditions.

Application to the Investigation of Hydrothermal Sn Species

Schmidt (2018, and references therein) showed that Sn-Cl complexes in hydrothermal solutions have characteristic Raman spectra for species with Sn in either the +2 (Sn^{II}) or +4 (Sn^{IV}) valence state. To demonstrate the current *in situ* redox control technique, a 0.5 *m* (mole/kg H_2O) $SnCl_4$ + 0.5 *m* HCl solution was sealed in an FSCC together with a vapour phase and exposed to a P_{H_2} of 0.2 bar in an HPOC after being heated to 300 °C (Fig. 1). Raman spectra of the solution were collected *in situ* under vapour saturation conditions as time elapsed from 0 to 156 hr (Fig. 3a).

The results show that all of the Sn was in the Sn^{IV} state at the beginning, and the amount of Sn^{II} species increased slowly with time up to 156 hr; at least 276 hr is needed to reach the reaction equilibrium (Figs. S-3, S-7). However, when the external P_{H_2} in the HPOC was increased to 1.3 bar, almost all of the Sn^{IV} were converted to Sn^{II} species within 48 hours (Fig. 3b); the tail around 321 cm^{-1} in the 48 hr spectrum may indicate a minor amount of remaining Sn^{IV}. Figure 4 shows *in situ* Raman spectra collected at various *T*s (30 to 300 °C) from an aqueous solution under vapour saturated pressures and an external P_{H_2} of 0.2 bar. For details see SI.

Deconvolution of Raman bands of $Sn^{II\,\&\,IV}$-Cl complexes collected at 30 °C before and after heating and reduction. Due to uncertain *T* effects on Raman shift for different $Sn^{II\,\&\,IV}$-Cl complexes, two spectra collected from the second FSCC sample solution at a constant temperature of 30 °C were selected for processing, in order to evaluate the contributions of different Sn-Cl complex species to the Raman bands before and after heating and reduction. Results were shown in Figure S-4; for details see SI.

Chemical vs. osmotic equilibrium. Our experimental results at 300 °C indicate that reaching chemical equilibrium in the Sn-H-Cl system requires a much longer time than that for the osmotic equilibrium for H_2 across the fused silica membrane (Figs. 2, 3). However, this conclusion is system specific and may not be valid for (a) other chemical systems, (b) the use of FSCC with different dimensions (*i.e.* OD, ID and length), or (c) other *P-T* experimental conditions. Therefore, more testing is required when applying this method.

The presence of unknown Sn^{IV} species between 30 and 75 °C. Figure S-5 shows that, at a constant *T* between 30 and 75 °C, the intensities of Raman spectroscopic band of Sn^{IV}-Cl species collected from an aqueous solution in an FSCC-containing 0.8 *m* $SnCl_4$ + 0.5 *m* HCl + 0.8 *m* NaCl during heating (blue) are lower than those collected during cooling (red). This may result from the presence of unknown Sn^{IV} species. For details, see SI.

Reduction kinetics of Sn^{IV}-Cl to Sn^{II}-Cl complexes at 300 °C. The reduction reaction of Sn^{IV}-Cl to Sn^{II}-Cl complexes at 300 °C under externally imposed P_{H_2} of 0.2 bar can be described by Eq. S-1, and the details on the derivation of reaction rate constant are given in SI.

Advantages of *In Situ* Observation and Raman Spectroscopic Characterisation

In situ observations show that the initial sample solution (0.5 *m* $SnCl_4$ + 0.5 *m* HCl) was a homogeneous solution at 25 °C,

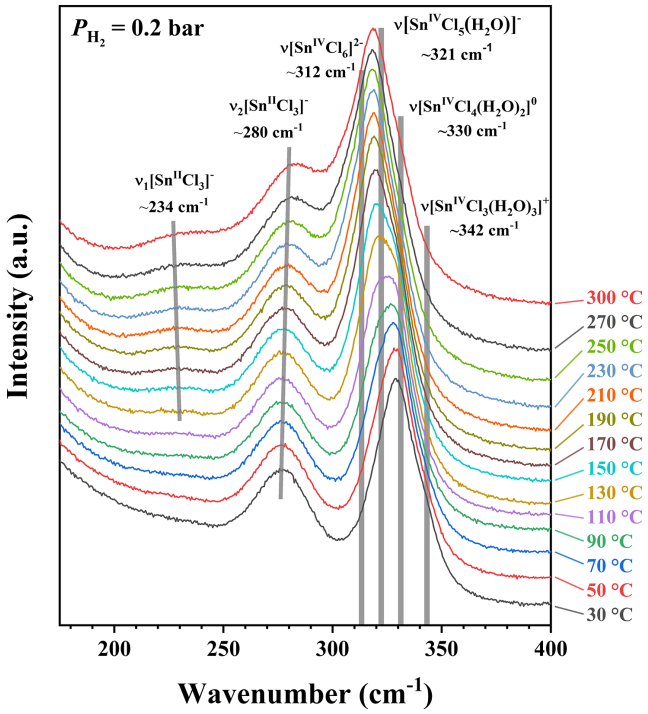

Figure 4 *In situ* Raman spectra collected at various *T*s (30 to 300 °C) from an aqueous solution under vapour saturated pressures and an externally imposed P_{H_2} of 0.2 bar. The sample initially contained 0.5 *m* $SnCl_4$ and 0.5 *m* HCl in an FSCC and was quenched from 300 °C after being kept at that *T* for 311 hr. Each spectrum was collected after the sample was kept at the specified *T* for at least 10 minutes, which were long enough for reaching equilibrium. The vertical gray lines were taken from Schmidt (2018), showing Raman peak positions of various Sn-bearing species at ambient *P-T* conditions.

presumably consisting mainly of Sn-Cl complexes and other unknown species, and they were saturated with respect to cassiterite at 125 °C (Fig. S-1a). However, the cassiterite precipitate could not be detected after being heated at 300 °C under an external P_{H_2} of 0.2 bar for 72 hours (Fig. S-1h), indicating that the formation and stabilisation of $Sn^{II\,\&\,IV}$-Cl complexes (and also the increase in acidity) increase the solubility of the cassiterite. These $Sn^{II\,\&\,IV}$-Cl complexes are still present after quenching (Fig. S-4b), and no cassiterite precipitation occurred during or after quenching. Even though these $Sn^{II\,\&\,IV}$-Cl complexes are quenchable, there is no guarantee that the proportions of these complexes remain the same. In contrast to the use of the conventional quench method for the study of cassiterite solubility, the coexistence of Sn^{II} and Sn^{IV} complexes and their quantities equilibrated at a specified *P-T*-pH-P_{H_2} experimental condition can be identified using our *in situ* method, when quantitative Raman spectroscopic analysis technique is eventually developed, such that the chemical equation for the dissolution of cassiterite in hydrothermal solutions can be correctly expressed.

Conclusions

Here we present an experimental technique for *in situ* redox control and Raman spectroscopic characterisation of complexes (*i.e.* $Sn^{II\,\&\,IV}$-Cl interactions) in vapour saturated aqueous solutions. We demonstrated that (a) the time required to reach osmotic equilibrium for H_2 across the fused silica membrane is shorter than that for chemical equilibrium between Sn^{II} and Sn^{IV}, (b) a 0.5 *m* $SnCl_4$ + 0.5 *m* HCl solution was saturated with respect to cassiterite (SnO_2) between 125 and 300 °C, before the species in the solution were converted to stable $Sn^{II\,\&\,IV}$-Cl complexes under an externally imposed P_{H_2} of 0.2 bar, and (c) the reduction rate from Sn^{IV}-Cl to Sn^{II}-Cl complexes at 300 °C under a P_{H_2} of 0.2 bar (equivalent to NNO buffer) was slow, but the rate increased substantially when P_{H_2} increased to 1.3 bar (equivalent to FMQ buffer). These findings are critical for the construction of a sound Sn mineralising mechanism. Furthermore, by using *in situ* Raman spectroscopic characterisation of the sample in an FSCC under a fixed *P-T* and redox state, we avoided the possible quench effects on the distribution of dissolved species and greatly increased our capabilities of performing rigorous hydrothermal experiments involving redox reactions at low temperatures, possibly even down to 200 °C (Fang and Chou, 2021).

Acknowledgements

We thank Dr. Y. Wan, Ms. Y. Chen and Ms. H.Y. Zhang in the Institute of Deep-sea Science and Engineering (IDSSE), the Chinese Academy of Sciences (CAS) for their assistance in our experiments. Constructive reviews were provided by Dr. Xiaolin Wang of Nanjing University, and Dr. Y. Wan and Dr. Nanfei Cheng of IDSSE, CAS. We thank Prof. Gleb Pokrovski and an anonymous reviewer for their critical and constructive reviews. This study was funded by the Key Frontier Science Program (QYZDY-SSW-DQC008) of CAS, and the National Natural Science Foundation of China (No. 41973055; No. 4213000358).

Editor: Satish Myneni

Additional Information

Supplementary Information accompanies this letter at https://www.geochemicalperspectivesletters.org/article2135.

Cite this letter as: Chou, I.-M., Wang, R., Fang, J. (2021) *In situ* redox control and Raman spectroscopic characterisation of solutions below 300 °C. *Geochem. Persp. Let.* 20, 1–5. https://doi.org/10.7185/geochemlet.2135

References

Alex, A., Zajacz, Z. (2020) A new method to quantitatively control oxygen fugacity in externally heated pressure vessel experiments. *European Journal of Mineralogy* 32, 219–234.

Berndt, J., Liebske, C., Holtz, F., Freise, M., Nowak, M., Ziegenbein, D., Hurkuck, W., Koepke, J. (2002) A combined rapid-quench and H_2-membrane setup for internally heated pressure vessels: Description and application for water solubility in basaltic melts. *American Mineralogist* 87, 1717–1726.

Chou, I.M. (1986) Permeability of precious metals to hydrogen at 2-Kb total pressure and elevated-temperatures. *American Journal of Science* 286, 638–658.

Chou, I.M. (1987) Calibration of the graphite-methane buffer using the fH_2 sensors at 2-kbar pressure. *American Mineralogist* 72, 76–81.

Chou, I.M., Song, Y.C., Burruss, R.C. (2008) A new method for synthesizing fluid inclusions in fused silica capillaries containing organic and inorganic material. *Geochimica et Cosmochimica Acta* 72, 5217–5231.

Eugster, H.P. (1957) Heterogeneous reactions involving oxidation and reduction at high pressures and temperatures. *Journal of Chemical Physics* 26, 1760–1761.

Fang, J., Chou, I.M. (2021) Redox control and measurement in low-temperature (< 450 °C) hydrothermal experiments. *American Mineralogist* 106, 1333–1340.

Matthews, W., Linnen, R.L., Guo, Q. (2003) A filler-rod technique for controlling redox conditions in cold-seal pressure vessels. *American Mineralogist* 88, 701–707.

Pokrovski, G.S., Dubrovinsky, L.S. (2011) The S_3^- ion is stable in geological fluids at elevated temperatures and pressures. *Science* 331, 1052–1054.

Pokrovski, G.S., Dubessy, J. (2015) Stability and abundance of the trisulfur radical ion S_3^- in hydrothermal fluids. *Earth and Planetary Science Letters* 411, 298–309.

Pokrovski, G.S., Kokh, M.A., Guillaume, D., Borisova, A.Y., Gisquet, P., Hazemann, J.-L., Lahera, E., Del Net, W., Proux, O., Testemale, D. (2015) Sulfur radical species form gold deposits on Earth. *Proceedings of the National Academy of Sciences* 112, 13484–13489.

Schmidt, C. (2018) Formation of hydrothermal tin deposits: Raman spectroscopic evidence for an important role of aqueous Sn(IV) species. *Geochimica et Cosmochimica Acta* 220, 499–511.

Shang, L.B., Chou, I.M., Lu, W.J., Burruss, R.C., Zhang, Y.X. (2009) Determination of diffusion coefficients of hydrogen in fused silica between 296 and 523 K by Raman spectroscopy and application of fused silica capillaries in studying redox reactions. *Geochimica et Cosmochimica Acta* 73, 5435–5443.

Shaw, H.R. (1963) Hydrogen-water vapor mixtures: Control of hydrothermal atmospheres by hydrogen osmosis. *Science* 139, 1220–1222.

Taylor, J., Wall, V., Pownceby, M. (1992) The calibration and application of accurate redox sensors. *American Mineralogist* 77, 284–295.

Geochemical Perspectives Letters

In situ redox control and Raman spectroscopic characterisation of solutions below 300 °C

I.-M. Chou, R. Wang, J. Fang

Supplementary Information

The Supplementary Information includes:

- S-1. Previous Redox Buffer Techniques Without Precious Metal Hydrogen Membranes
- S-2. Optical Cell Setup and Sample Preparation
- S-3. Collection and Processing of Raman Spectra
- S-4. Temperature Effect on the Sn-Cl Complexes in a Vapour-saturated Sn-H-Cl Aqueous Solution
- S-5. Deconvolution of Raman Bands of $Sn^{II\ \&\ IV}$-Cl Complexes Collected at 30 °C Before and After Heating and Reduction
- S-6. The Presence of Unknown Sn^{IV} Species between 30 and 75 °C
- S-7. Reduction Kinetics of Sn^{IV}-Cl to Sn^{II}-Cl Complexes at 300 °C
- Figures S-1 to S-7
- Supplementary Information References

S-1. Previous Redox Buffer Techniques Without Precious Metal Hydrogen Membranes

To control the redox state of a sample in a hydrothermal experiment without using precious metal hydrogen membrane, many techniques have been applied, and they can be grouped into three categories (Fang and Chou, 2021): (1) loading a solid oxygen buffer together with studied samples without physical separation by a membrane (*e.g.*, Gibert *et al.*, 1998; Seewald, 2001; Tagirov *et al.*, 2005; Kokh *et al.*, 2017); (2) introducing a quartz tube oxygen buffer holder with one end sealed and the open end exposed to the vapour phase of the sample in an autoclave (*e.g.*, Archibald *et al.*, 2001; Timofeev *et al.*, 2018; Shang *et al.*, 2020); and (3) attaining internal redox equilibrium of multivalent species (*e.g.*, sulfur species) included in the studied system (*e.g.*, Pokrovski *et al.*, 2015; Kokh *et al.*, 2020).

S-2. Optical Cell Setup and Sample Preparation

A schematic diagram of the experimental setup is shown in Figure 1. A sample solution was loaded and sealed together with a vapour phase in an FSCC [150 μm inner diameter (ID), 375 μm outer diameter (OD) and ~ 6 mm long] following the procedures of Chou *et al.* (2008). This FSCC was then inserted in an HPOC (450 μm ID, 670 μm OD and ~17 cm long), which was then connected to a *P* line through a high-*P* valve (HiP 15-15AF1). The connected HPOC and *P* line were then vacuumed and flushed with H_2 (99.999 % from Guangdong Huate Gas Co.) three times before loading H_2, and its *P* was adjusted with a *P* generator and measured using a *P* transducer (25 psi in full scale and accurate to ±0.25 % of the full scale; Setra Systems, Inc.). The sample in the FSCC was heated to a fixed *T* on a heating-cooling stage (Linkam CAP500) and exposed to a fixed external P_{H_2} either during heating or after it reached the target *T*. The reported *T* has an accuracy of ±0.1 °C from 0 to 100 °C, which gradually increases to ±0.3 °C at 300 °C (Chen and Chou, 2020).

The used chemical reagents include $SnCl_4 \cdot 5H_2O$ crystals (98 %, Acros-Organics), hydrochloric acid (Analytical reagent, Xilong Scientific Co., Ltd.) and deionised H_2O (via a Millipore water filtration system; 18.24 MΩ·cm). A solution containing 0.5 *m* (mole/kg H_2O) $SnCl_4$ + 0.5 *m* HCl was then prepared and sealed in an FSCC, following the method of Chou *et al.* (2008), with the solution occupying approximately half of the available volume in the FSCC, such that the bulk density of the solution in the FSCC was approximately 0.5 g/ml and the solution was under vapour-saturation *P*s at experimental *T*s below 300 °C. Note that, in the preparation of the experimental system shown in Figure 2a, a short fused silica capillary tube with the same ID and OD as the FSCC, but with two ends open, was inserted in the HPOC (inner tube 2 in Fig. 2a). Because the intensity of a Raman band, such as the peak height, collected through two layers of fused silica will be lower than that collected through only one layer, therefore, it was necessary to insert inner tube 2 to yield the Raman signals of the external H_2 through two layers of fused silica, to be fairly compared with those collected from the FSCC.

S-3. Collection and Processing of Raman Spectra

A JY/Horiba LabRAM HR Evolution Raman spectrometer was applied to acquire the Raman spectra using a 532.06 nm (Nd: YAG) laser, a super-long-working-distance 50× Olympus objective with a 0.35 numerical aperture, and an 1800 groove/mm grating with a spectral resolution of approximately 0.65 cm^{-1}.

Approximately 14 mW of the laser light was focused near the center of the sample cell to generate the Raman signals during measurement. The peak heights of H_2 (PH_{H_2}) were calculated with an in-house program, similar to the GRAM32/AI software (used in Fang and Chou, 2021), and are available on request. Note that baseline removing process of spectra was done through the Labspec 5 software with a linear equation, and that a Peakfit 4.0 software and Gaussian-Lorentzian area function were used to deconvolute these spectroscopic bands. It was assumed that the quantities of Sn-Cl species were directly related to their peak areas.

S-4. Temperature Effect on the Sn-Cl Complexes in a Vapour-saturated Sn-H-Cl Aqueous Solution

To examine the *T* effect on the phase relations and Sn-Cl complexes in a vapour-saturated Sn-H-Cl aqueous solution, another FSCC was prepared from the same aqueous solution initially containing 0.5 *m* $SnCl_4$ and 0.5 *m* HCl. This FSCC was heated slowly, and many small particles were observed precipitating at ~125 °C (Fig. S-1a), which became larger in size and number at 300 °C (Fig. S-1b). This sample was cooled to 25 °C, and the precipitates were centrifuged to one end of the FSCC before being heated again to 300 °C (Fig. S-1c). The sample was kept at 300 °C for 3 hours, and crystals grew from these precipitates (Fig. S-1d), yielding the characteristic Raman peak of cassiterite at ~635 cm^{-1} (Scott, 1970; Fig. S-2). At this point, 0.2 bar of the external P_{H_2} was applied to the FSCC (Fig. S-1e). Cassiterite crystals could still be observed up to 56 hr (Figs. S-1f, g) but were not detected at 72 hr (Fig. S-1h). The *in situ* Raman spectra were then collected at 300 °C from the homogeneous fluid from time to time up to 311 hr under the vapour saturation *P*. The results (Fig. S-3) showed that about 276 hours are needed to reach the steady state distribution of Sn^{II} and Sn^{IV} species in the solution under the set P-T-P_{H_2} condition. It should be noted that the steady state was not reached at the reaction time of 156 hr (Fig. 3a, which is presented as a black dashed line in Fig. S-3). This sample was then quenched, and *in situ* Raman spectra were collected at various *T*s during heating from 30 to 300 °C under an externally imposed P_{H_2} of 0.2 bar, as shown in Figure 4. The spectrum was collected after the sample was kept at the specified *T* for at least 10 minutes. In our preliminary experiment, we found that the rates of conversions among $Sn^{II\ \&\ IV}$-Cl complexes in response to temperature change were fast (less than 5 min), which were much faster than those for reducing Sn^{IV}-Cl complexes to Sn^{II}-Cl complex under 0.2 bar of H_2. When the sample *T* was increased from 30 to 300 °C, the observed ~12 cm^{-1} low-wavenumber shift of Sn^{IV}-Cl complexes peak is in agreement with that reported by Schmidt (2018; Fig. 3 within the

paper). Note that the redox control was not ensured in Schmidt (2018), and that the presence of Sn^{II} in the study may be caused by the presence of contaminating H_2, which was produced by the reaction between diamond and H_2O catalyzed by the Ir gasket used in the study (see Fig. 1d and Table 1 of Chou and Anderson, 2009).

S-5. Deconvolution of Raman Bands of $Sn^{II\ \&\ IV}$-Cl Complexes Collected at 30 ˚C Before and After Heating and Reduction

Results of deconvolution of Raman spectroscopic bands of Sn^{IV}-Cl complexes collected at 30 ℃ from the second FSCC sample solution, initially containing 0.5 *m* $SnCl_4$ + 0.5 *m* HCl, under vapour-saturated pressure before further heating and H_2 exposure are shown in Figure S-4a, and those for $Sn^{II\ \&\ IV}$-Cl complexes after exposure to 0.2 bar of P_{H_2} at 300 ℃ for 311 hr (see Fig. S-3) are shown in Figure S-4b. Results show that the Sn^{IV}-Cl band was composed of 55 % $Sn^{IV}Cl_5(H_2O)^-$, 26 % $Sn^{IV}Cl_4(H_2O)_2^0$ and 19 % $Sn^{IV}Cl_3(H_2O)_3^+$ before heating and reduction (Fig. S-4a), and was changed to 24 %, 60 %, and 16 %, respectively, after heating and reduction (Fig. S-4b). These results imply that $Sn^{IV}Cl_5(H_2O)^-$ was possibly the main species being reduced in the initial solution at 300 °C under an externally imposed P_{H_2} of 0.2 bar.

S-6. The Presence of Unknown Sn^{IV} Species between 30 and 75 °C

A 3rd FSCC sample, containing 0.8 *m* $SnCl_4$ + 0.5 *m* HCl + 0.8 *m* NaCl solution and a vapour phase, was prepared for comparing Raman spectra collected during heating and cooling. During heating at the rate of 5 °C/min, cassiterite precipitated at about 125 °C, started to dissolve at about 225 °C, and was totally dissolved at 275 °C within one hour. After heating to 300 °C, the sample solution was then quickly quenched to 75 °C and slowly cooled down to 30 °C. No cassiterite was observed to precipitate during this cooling process, while a series of Raman spectra was collected. Figure S-5 shows that the intensities of Sn^{IV}-Cl complexes Raman bands collected during heating were obviously lower than those collected during cooling. Because there was no visible precipitation during the collection of these spectra, total Sn concentrations in all of these solutions remained the same. Therefore, at the same temperature (between 30 and 75 °C), the lower intensities of the Sn^{IV}-Cl complexes Raman bands collected during heating was possibly due to (1) the presence of unknown Sn^{IV} species, and (2) the slow decomposition rate of Sn^{IV}-Cl species at temperatures between 30 and 75 °C after they were formed at 300 °C.

S-7. Reduction Kinetics of Sn^{IV}-Cl to Sn^{II}-Cl Complexes at 300 °C

The reduction reaction of Sn^{IV}-Cl to Sn^{II}-Cl complexes at 300 °C under externally imposed P_{H_2} of 0.2 bar can be described by:

$$[Sn^{IV}Cl_n]^{4-n} + H_2 = [Sn^{II}Cl_3]^- + 2\,H^+ + (n-3)\,Cl^- \qquad \text{(Eq. S-1)}$$

where n = 3 to 6. According to Eq. S-1, the kinetic model rate equation of Sn^{IV}-Cl complexes reduction is expressed as:

$$-\frac{d[Sn^{IV}]}{dt} = k[Sn^{IV}][H_2] \qquad \text{(Eq. S-2)}$$

where k and t are the reaction rate constant and time, respectively, $[Sn^{IV}]$ is the total concentration of all Sn^{IV}-Cl complexes, including $Sn^{IV}Cl_6(H_2O)^{2-}$, $Sn^{IV}Cl_5(H_2O)^-$, $Sn^{IV}Cl_4(H_2O)_2^0$ and $Sn^{IV}Cl_3(H_2O)_3^+$, and $[H_2]$ is H_2 pressure. Because H_2 pressure was fixed at 0.2 bar during the reaction, therefore Eq. S-2 becomes:

$$-\frac{d[Sn^{IV}]}{dt} = k'[Sn^{IV}] \qquad \text{(Eq. S-3)}$$

where $k' = k[H_2] = 0.2\,k$.

Assuming that the initial total concentration of Sn^{IV}-Cl complexes is $[Sn^{IV}]_0$, and the total concentration of all Sn^{IV}-Cl complexes that have not been reduced in time t is $[Sn^{IV}]_t$, Eq. S-3 can be converted to :

$$\ln\frac{[Sn^{IV}]_0}{[Sn^{IV}]_t} = k't \qquad \text{(Eq. S-4)}$$

To minimize the instrumental effects of Raman system, Eq. S-4 is converted to:

$$\ln\frac{PAR_0}{PAR_t} = k't \qquad \text{(Eq. S-5)}$$

where PAR_0 and PAR_t are Raman peak area ratios between Sn^{IV}-Cl band and water band at time 0 and t, respectively. For example, Figure S-6 shows *PAR* for t = 0 and 229 hr, and the calculated data points are marked by red circles in Figure S-7, in which the slope of the black line represents the rate coefficient $\boldsymbol{k'}$. The rate coefficient $\boldsymbol{k'}$ of 0.0045 (h^{-1}) at 300 °C was obtained based on the data collected from the 2nd FSCC sample shown in Figure S-3. In the same manner, the rate coefficients $\boldsymbol{k'}$ calculated from the generated amount of Sn^{II}-Cl complex based on the *PAR* derived from $\nu_1[Sn^{II}Cl_3^-]$ band (~230 cm^{-1}) and $\nu_2[Sn^{II}Cl_3^-]$ band (~280 cm^{-1}) were 0.0046 and 0.0049 (h^{-1}), respectively, and they were in good agreement with 0.0045 (h^{-1}) derived from the Raman band of Sn^{IV}-Cl complexes described above.

Supplementary Figures

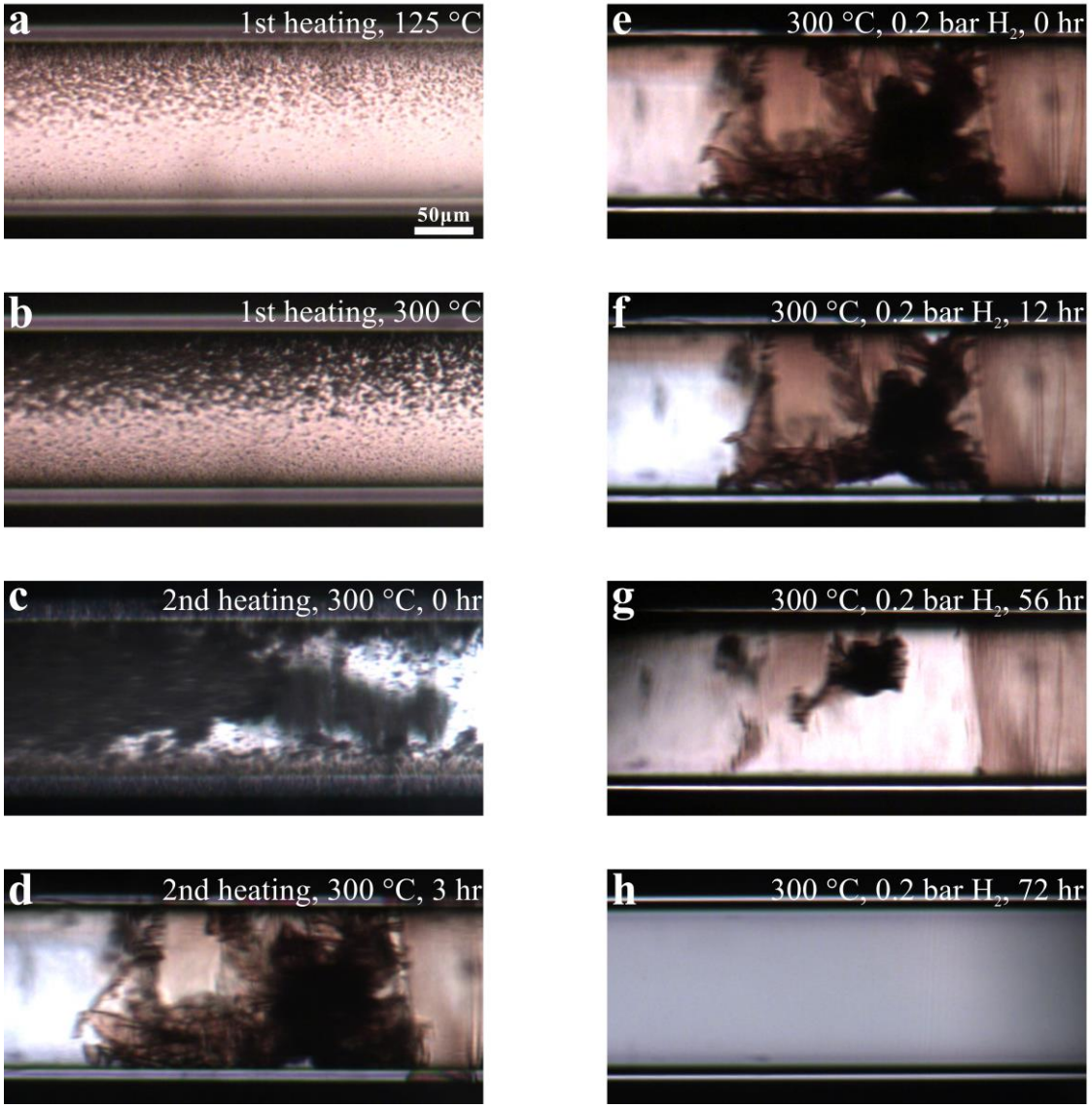

Figure S-1 Photomicrographs of an FSCC, initially containing 0.5 *m* $SnCl_4$ and 0.5 *m* HCl, taken at elevated *T*s under vapour-saturated *P*s without **(a-d)** and with **(e-h)** an externally imposed P_{H_2} of 0.2 bar. Initial precipitates were observed at approximately 125 °C **(a)**, and *in situ* Raman analysis of the crystals in **(d)** indicates that they were cassiterite (Fig. S-2), which could not be detected at 300 °C after being exposed to a P_{H_2} of 0.2 bar for 72 hours **(hr)**. For details, see the text. A scale bar is shown in **(a)**.

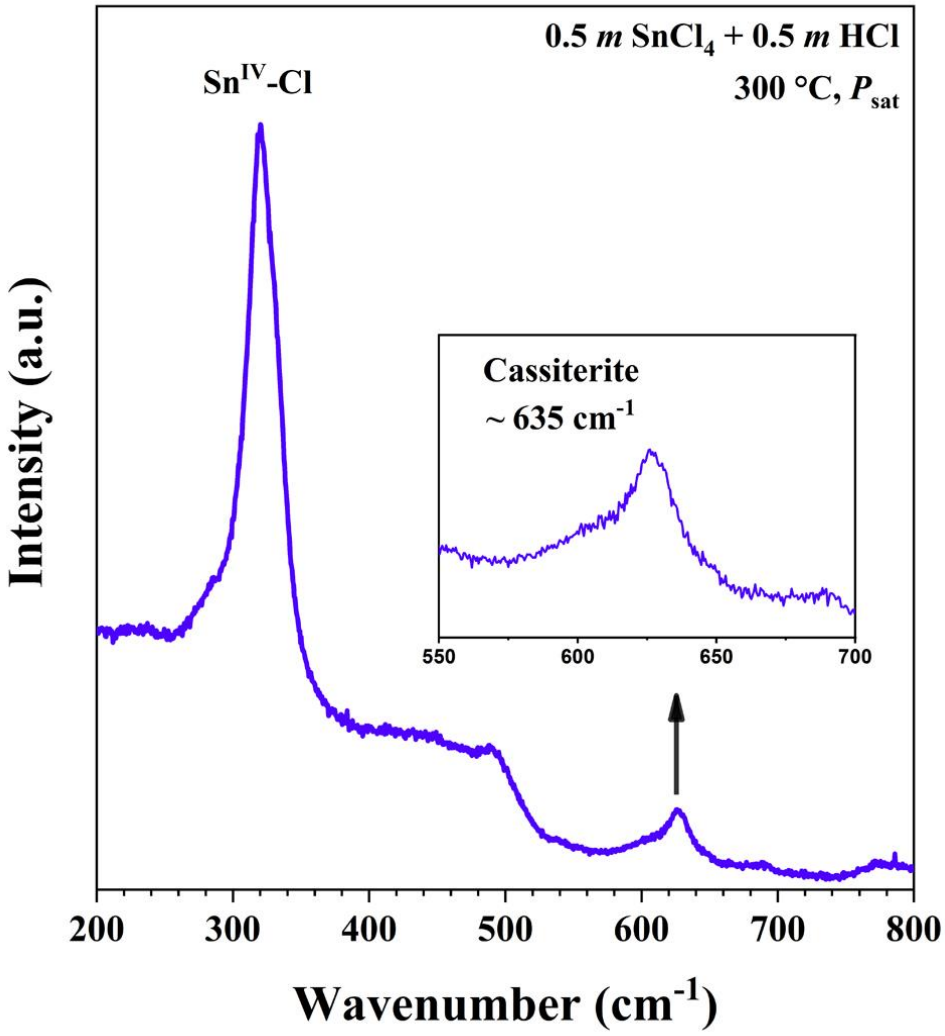

Figure S-2 *In situ* Raman spectrum collected from crystals shown in Figure S-1d. The insert shows the characteristic peak of cassiterite near 635 cm^{-1} (Scott, 1970). P_{sat} = vapour-saturated P.

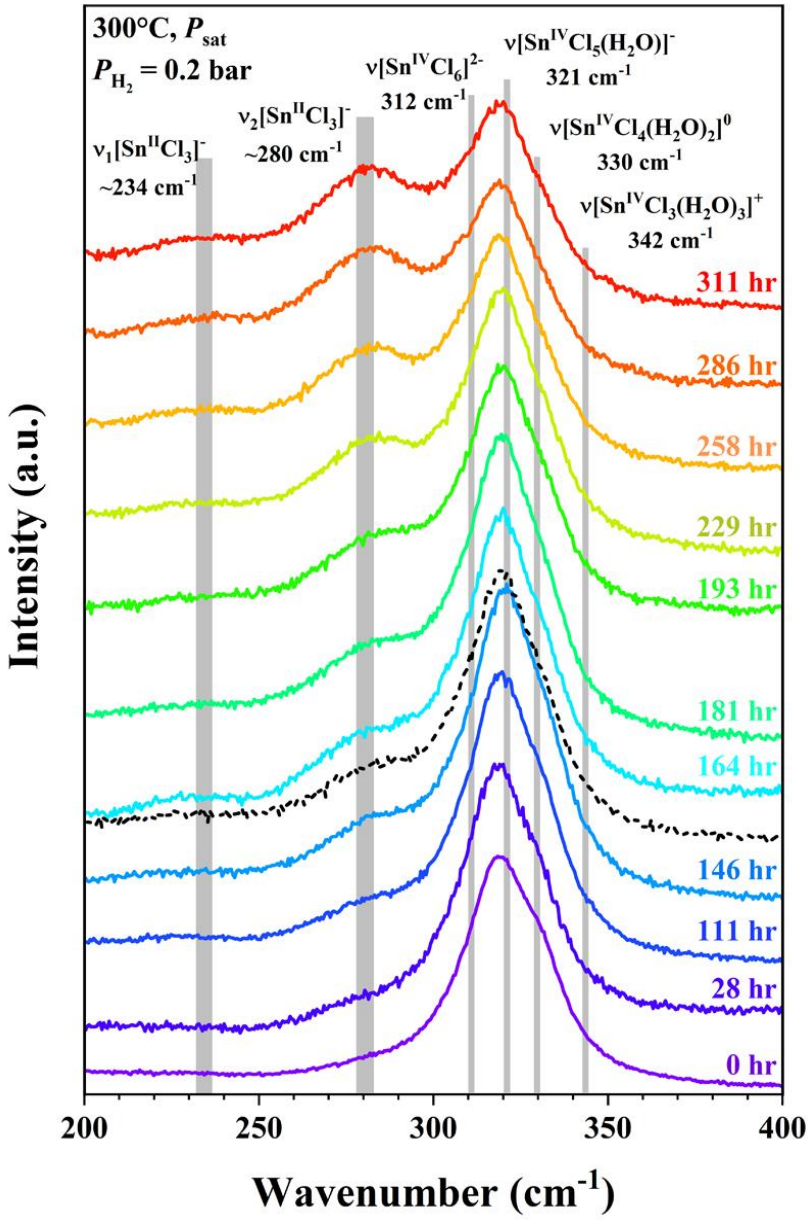

Figure S-3 *In situ* Raman spectra collected from the second FSCC sample (0.5 *m* $SnCl_4$ + 0.5 *m* HCl initial solution) at 300 °C under vapour-saturated *P* (P_{sat}) and an externally imposed P_{H_2} of 0.2 bar for durations up to 311 hours. For clarity, not all spectra are shown. For comparison, the spectrum collected at 156 hr shown in Figure 3a is presented here as the black dashed line, indicating that the system had not reached a steady state at that time. The vertical gray lines were taken from Schmidt (2018), showing Raman peak positions of various Sn-Cl species at ambient *P*-*T* conditions.

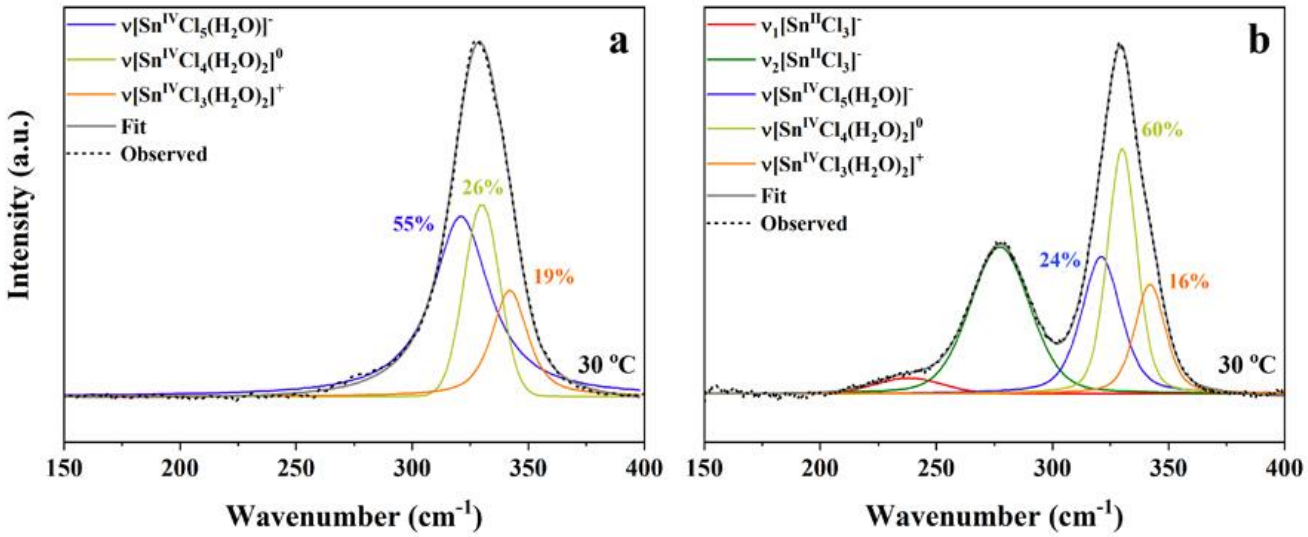

Figure S-4 Deconvolution of Raman bands of $Sn^{II\ \&\ IV}$-Cl complexes collected at 30 °C from the second FSCC sample solution initially containing 0.5 *m* $SnCl_4$ + 0.5 *m* HCl under vapour-saturated pressure (**a**) before further heating and H_2 exposure, and (**b**) after exposure to 0.2 bar of P_{H_2} at 300 °C for 311 hr (see Fig. S-3). No cassiterite precipitation was observed during the collection of both spectra. The marked percentages are for the Sn^{IV}-Cl complexes only.

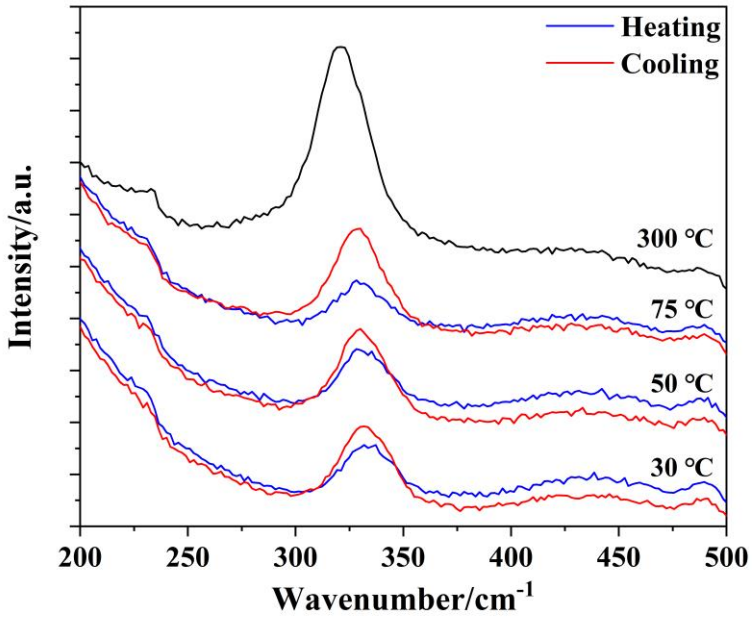

Figure S-5 Comparison of Raman bands of Sn^{IV}-Cl species collected from an aqueous solution in an FSCC containing 0.8 *m* $SnCl_4$ + 0.5 *m* HCl + 0.8 *m* NaCl during heating and cooling. Cassiterite precipitated at about 125 °C during heating (5 °C/min), then started to dissolve at about 225 °C and totally dissolved at 275 °C within one hour. There was no visible precipitation during the collection of all presented spectra. Raman intensities of the Sn^{IV}-Cl complex bands collected during heating (blue) were obviously lower than those collected during cooling (red), indicating the presence of unknown Sn^{IV} species.

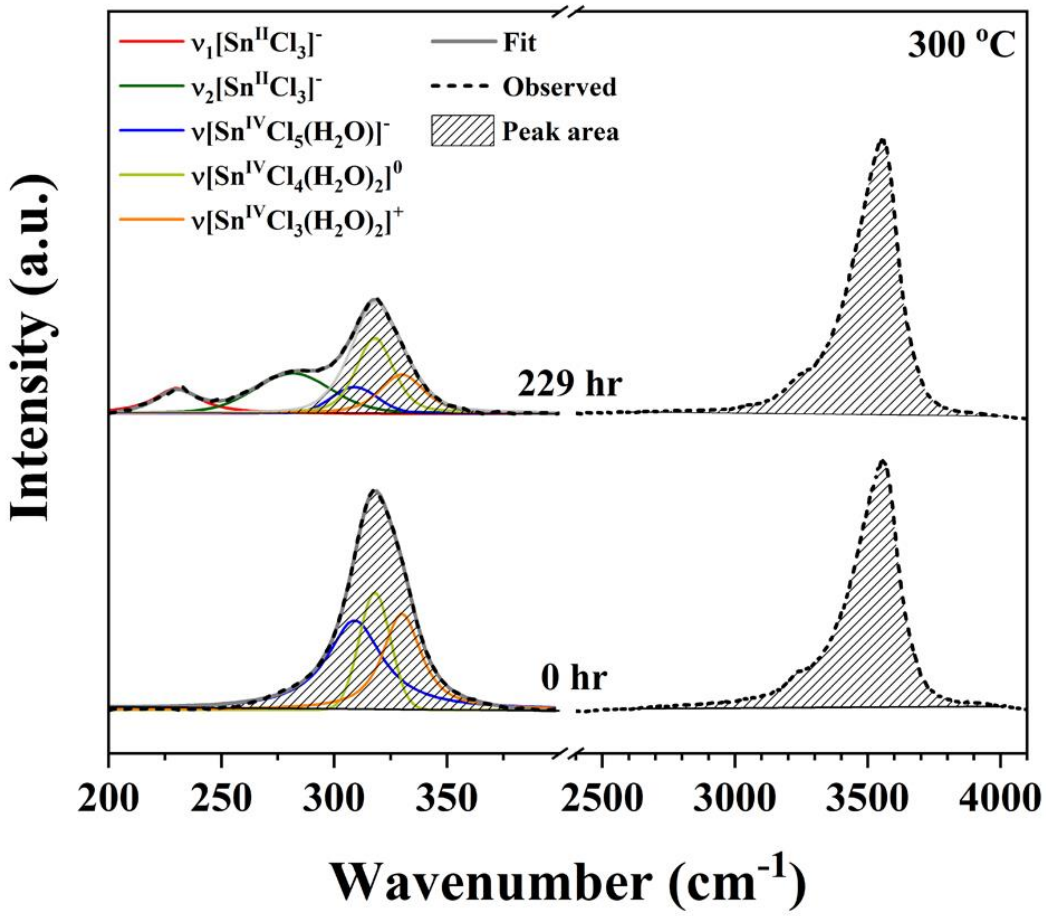

Figure S-6 Deconvolution of Raman spectroscopic bands of $Sn^{II\ \&\ IV}$-Cl complexes in two spectra collected from the second FSCC sample solution (initially containing 0.5 *m* $SnCl_4$ + 0.5 *m* HCl) at 300 °C under vapour-saturated *P* before (0 hr; lower spectrum below 400 cm^{-1}) and after being exposed to P_{H_2} of 0.2 bar for 229 hr (upper spectrum below 400 cm^{-1}). Also shown are the peak areas of Sn^{IV}-Cl complexes bands (ruled area below 400 cm^{-1}) together with those of H_2O band (ruled area between 2500 and 4000 cm^{-1}). The peak area ratios (*PAR*) between Sn^{IV}-Cl complexes band and H_2O band were calculated for time 0 and 229 hr and plotted in Figure S-7 (marked by red circles).

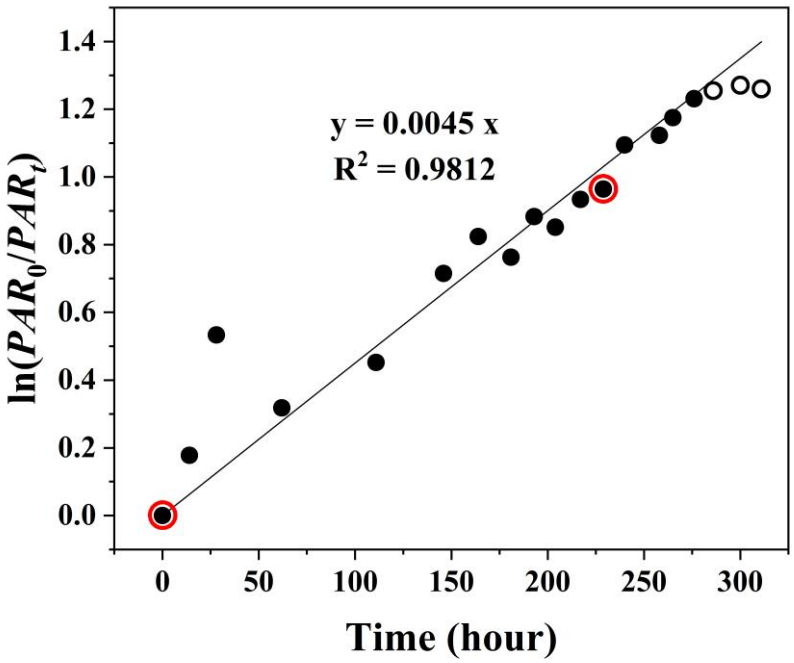

Figure S-7 Relationship between ln(PAR_0/PAR_t) and reaction time. Linear regression of the data shown by black dots yields the black line, the slop of which represents the rate coefficient, $\boldsymbol{k'}$. The three open black circles represent data points at 286, 300, and 311 hr; they were not included in linear regression as no further reduction was detected after 276 hr. The two data points enclosed by red circles were derived from Figure S-6 at 0 and 229 hr.

Supplementary Information References

Archibald, S.M., Migdisov, A.A., Williams-Jones, A.E. (2001) The stability of Au-chloride complexes in water vapor at elevated temperatures and pressures. *Geochimica et Cosmochimica Acta* 65, 4413–4423.

Chen, Y., Chou, I.M. (2020) Measurements of vapor pressures of aqueous solutions in the NaCl–KCl–H_2O system from 493.15 to 693.25 K in a fused silica capillary high-pressure optical cell. *Journal of Chemical & Engineering Data* 65, 766-776.

Chou, I.M., Anderson,A.J. (2009) Diamond dissolution and the production of methane and other carbon-bearing species in hydrothermal diamond-anvil cells. *Geochimica et Cosmochimica Acta* 73, 6360–6366.

Chou, I.M., Song, Y.C., Burruss, R.C. (2008) A new method for synthesizing fluid inclusions in fused silica capillaries containing organic and inorganic material. *Geochimica et Cosmochimica Acta* 72, 5217–5231.

Fang, J., Chou, I.M. (2021) Redox control and measurement in low-temperature (< 450 °C) hydrothermal experiments. *American Mineralogist* 106, 1333–1340.

Gibert, F., Pascal, M.L., Pichavant, M. (1998) Gold solubility and speciation in hydrothermal solutions: experimental study of the stability of hydrosulphide complex of gold (AuHS°) at 350 to 450°C and 500 bars. *Geochimica et Cosmochimica Acta* 62, 2931–2947.

Kokh, M.A., Akinfiev, N.N., Pokrovski, G.S., Salvi, S., Guillaume, D. (2017) The role of carbon dioxide in the transport and fractionation of metals by geological fluids. *Geochimica et Cosmochimica Acta* 197, 433–466.

Kokh, M.A., Assayag, N., Mounic, S., Cartigny, P., Gurenko, A., Pokrovski, G.S. (2020) Multiple sulfur isotope fractionation in hydrothermal systems in the presence of radical ions and molecular sulfur. *Geochimica et Cosmochimica Acta* 285, 100–128.

Pokrovski, G.S., Kokh, M.A., Guillaume, D., Borisova, A.Y., Gisquet, P., Hazemann, J.L., Lahera, E., Del Net, W., Proux, O., Testemale, D. (2015) Sulfur radical species form gold deposits on Earth. *Proceedings of the National Academy of Sciences* 112, 13484–13489.

Schmidt, C. (2018) Formation of hydrothermal tin deposits: Raman spectroscopic evidence for an important role of aqueous Sn(IV) species. *Geochimica et Cosmochimica Acta* 220, 499–511.

Scott, J. (1970) Raman spectrum of SnO_2. *Journal of Chemical Physics* 53, 852–853.

Seewald, J.S. (2001) Aqueous geochemistry of low molecular weight hydrocarbons at elevated temperatures and pressures: constraints from mineral buffered laboratory experiments. *Geochimica et Cosmochimica Acta* 65, 1641–1664.

Shang, L.B., Williams-Jones, A.E., Wang, X.S., Timofeev, A., Hu, R.Z., Bi, X.W. (2020) An experimental study of the solubiliy and speciation of MoO_3(s) in hydrothermal fluids at temperature up to 350°C. *Economic Geology* 115, 661–669.

Tagirov, B.R., Salvi, S., Schott, J., Baranova, N.N. (2005) Experimental study of gold-hydrosulphide complexing in aqueous solutions at 350–500°C, 500 and 1000 bars using mineral buffers. *Geochimica et Cosmochimica Acta* 69, 2119–2132.

Timofeev, A., Migdisov, A.A., Williams-Jones, A.E., Roback, R., Nelson, A.T., Xu, H. (2018) Uranium transport in acidic brines under reducing conditions. *Nature Communications* 9, 1–7.